Journal of Southeast University (English Edition) Vol. 25, No. 1, pp. 83 – 88 Mar. 2009 ISSN 1003—7985

# Measurement and analysis of defects in high-performance concrete with three-dimensional micro-computer tomography

Guo Liping[1,2] Andrea Carpinteri[3] Sun Wei[1,2] Qin Wenchao[4]

([1]School of Materials Science and Engineering, Southeast University, Nanjing 211189, China)
([2]Jiangsu Key Laboratory of Construction Materials, Southeast University, Nanjing 211189, China)
([3]Department of Civil Engineering, University of Parma, Parma 43100, Italy)
([4]YXLON International X-Ray GmbH Shanghai Rep. Office, Shanghai 200041, China)

**Abstract:** In order to investigate the effects of two mineral admixtures (i. e., fly ash and ground slag) on initial defects existing in concrete microstructures, a high-resolution X-ray micro-CT (micro-focus computer tomography) is employed to quantitatively analyze the initial defects in four series of high-performance concrete (HPC) specimens with additions of different mineral admixtures. The high-resolution 3D images of microstructures and filtered defects are reconstructed by micro-CT software. The size distribution and volume fractions of initial defects are analyzed based on 3D and 2D micro-CT images. The analysis results are verified by experimental results of water-suction tests. The results show that the additions of mineral admixtures in concrete as cementitious materials greatly change the geometrical properties of the microstructures and the spatial features of defects by physical-chemistry actions of these mineral admixtures. This is the major cause of the differences between the mechanical behaviors of HPC with and without mineral admixtures when the water-to-binder ratio and the size distribution of aggregates are constant.

**Key words:** high-performance concrete; defect; microstructure; X-ray micro-focus computer tomography; mineral admixtures

Apart from coarse or fine aggregates in concrete, the cracks, voids and porosities (collectively called defects) are the most remarkable weak components in concrete microstructures. Furthermore, spatial distributions and volume fractions of initial defects are essential for agent transport, mechanical performance and durability of concrete or concrete structures[1-2]. Most of the investigations on microstructures of hardened concrete are only based on comparisons of different 2D slice images captured by an optical/electrical microscope. ASTM-C457[3] recommends the microscopic determination method to measure the air-voids system in hardened concrete. Unfortunately, the spatial parameters have to be determined from a series of regularly spaced lines traversed on finely ground slices of hardened concrete[1]. However, only 2D parameters of defects in concrete microstructures are not enough for a comprehensive understanding and prediction of micro-crack growth and its influence on properties of bulk concrete. Since the experimental methods for detecting the three-dimensional microstructure data were not advanced enough in past decades, previous researches in this field employed numerical modeling to understand and predict the bulk failure response of concrete based on simulated microstructural data[4-6].

In the last decade, X-ray computer tomography (CT) has been employed for scanning concrete microstructure and for analyzing air voids or cracks. The detailed CT principles can be found in Ref. [7]. Flannery and coworkers[8] developed a matched algorithm to reconstruct three-dimensional X-ray micro-tomography images. Landis and coworkers[9] took the first step on quantitative analysis of three-dimensional crack geometry in concrete by the use of X-ray CT. Wong and Chau[1] used the X-ray CT to examine the evolution of air voids inside high-performance concrete under uniaxial compression based on reconstructed 2D CT scan images, but they did not show 3D distribution images and diameter distributions of defects inside hardened concrete. Zhang and coworkers[10] made many researches on fracture energy of concrete using 3D X-ray micro-CT images, and improved on the analysis method of 3D micro-CT images to investigate the defect properties in a more powerful way.

However, all of the previous researchers did not further discuss the effects of material admixtures (e. g. ground slag and fly ash) on the spatial information of defects existing in concrete microstructures.

Therefore, this paper aims at investigating the effects of fly ash and ground granulated blast-furnace slag on 3D parameters of initial defects inside hardened high-performance concrete (HPC). It is known that the image resolution governs the accuracy of analysis results of these defects. A high-resolution X-ray micro-CT is employed in the present work to scan each concrete specimen and reconstruct 3D images in about 300 s. The 3D image reconstruction is conducted by the combination-weighted Feldkamp-based reconstruction algorithm[11], the noise filter arithmetic, and the internal geometrical compensation technique.

## 1 Experimental Preparation

### 1.1 Specimens

Concrete cubes with 100 mm side lengths are cast for four different batches (RC, S5, F3 and F2S3). RC is the reference concrete without any mineral admixtures. S5 is the concrete with a 50% mass fraction of ground slag in total cementitious materials. F3 is the concrete with a 30% mass fraction

**Received** 2008-07-20.

**Biographies:** Guo Liping (1979—), female, doctor, lecturer, guoliping@seu.edu.cn; Sun Wei (1935—), female, doctor, professor, academician of China Engineering Academy, sunwei@seu.edu.cn.

**Foundation items:** The Scholarship Supported by Ministry of Education of China for Research Abroad (No. 3037 [2006]), the Excellent Doctoral Dissertation Foundation of Southeast University (No. YBTJ-0512), the National Basic Research Program of China (973 Program) (No. 2009CB623203).

**Citation:** Guo Liping, Andrea Carpinteri, Sun Wei, et al. Measurement and analysis of defects in high-performance concrete with three-dimensional micro-computer tomography[J]. Journal of Southeast University (English Edition), 2009, 25(1): 83 – 88.

of fly ash in total cementitious materials. F2S3 is the concrete with a 20% mass fraction of fly ash and a 30% mass fraction of ground slag in total cementitious materials. As shown in Tab. 1, the material components are a little different among the four batches. But the water-to-binder ratio (the ratio of water and total cementitious materials by weight) of 0. 35, the sand percentage (sand to total aggregate ratio by weight) of 0. 38, and the coarse aggregate to binder ratio (the ratio of coarse aggregate and total cementitious materials by weight) of 2. 4 are kept constant by weight for all batches of concrete. The main cementitious material used in this research is CEM Ⅱ/A 42. 5 Portland cement. Class F of fly ash with a density of 2 380 kg/m$^3$ and S95 ground slag with a density of 2 860 kg/m$^3$ are mixed into three batches as a part of the cementitious materials. The specific surface area is 665 m$^2$/kg for fly ash and 372 m$^2$/kg for ground slag. Natural river sand and crushed basalt aggregate are used as fine and coarse aggregates, respectively. The size range is from 0. 15 to 4. 75 mm for sand and 5 to 20 mm for coarse aggregates with a continuous grading. The tap water with a pH value of 8 to 10 is used for casting the concrete. The dosage of naphthalene super-plasticizer in concrete is 0. 5% to 1% of the total weight of cementitious materials.

**Tab. 1** Mix designs of four concrete series kg/m$^3$

| Content | RC | S5 | F3 | F2S3 |
|---|---|---|---|---|
| Cement | 460 | 230 | 322 | 230 |
| Water | 161 | 161 | 161 | 161 |
| Fly ash | 0 | 0 | 138 | 92 |
| Ground slag | 0 | 230 | 0 | 138 |
| Natural river sand | 676 | 676 | 676 | 676 |
| Crushed basalt aggregate | 1104 | 1104 | 1104 | 1104 |

The slumps of the fresh concrete pastes are controlled to be in the range of 8 to 12 cm by adjusting the dosage of super-plasticizer. All cubes are cast in steel moulds in the lab at a temperature of 20 ℃ and air-cured for 24 h. Then they are demoulded and cured at (20 ± 2) ℃ with more than 90% relative humidity for three months. Since the fly ash and ground slag are mixed into the concrete as a part of the cementitious materials, the specimens with a hydration age of 90 d are ordered for mechanical tests according to Test Code for Hydro-Concrete (DL/T 5150—2001). The compressive strengths and the 4-point flexural strengths for the four concrete series with hydration age of 90 d are presented in Tab. 2. The compressive strengths of series RC and F3 are higher than 80 MPa, and those of series S5 and F2S3 are around 70 MPa. The flexural strength of F3 is the highest among the four concrete series. Other performances of HPC with fly ash or ground slag under different mechanical loads or environmental effects were also reported in published literature[12-13]. From these research results, it has been confirmed that the mechanical behavior of concrete is obviously changed by the admixtures of ground slag and fly ash when the water-to-binder ratio and size distribution of aggregates are constant. Since the matrix-aggregate interfacial transition zone (ITZ) is the most complex and weakest constituent in concrete microstructures, the mechanical behavior of concrete is greatly influenced by the properties (such as density and tensile strength) of the matrix-aggregate ITZ. Furthermore, the microstructures of this ITZ change with the type and dosage of mineral admixtures and they also change with the water-to-cement ratio. In the present study, the water-to-cement ratios of the four concrete series are constant and equal to 0. 35. Therefore, the additions of different mineral admixtures with various dosages in concrete are the only probable reasons for any changes in the mechanical behavior of HPC. After adding FA and GGBS in the concrete as a part of cementitious materials, the densities of the matrix-aggregate ITZ with them are changed because of the micro-filling effect (contributed by the fine shape and high stiffness of FA grains) of FA as well as the pozzolanic effect (supported with the reaction of $SiO_2$ in FA/GGBS grain with $Ca(OH)_2$ in solution) of FA and GGBS[14]. Furthermore, the compressive strength and the tensile strength of HPC also change with the dosages of FA and GGBS.

**Tab. 2** Compressive strength and flexural strength of concrete with hydration age of 90 d MPa

| Item | RC | S5 | F3 | F2S3 |
|---|---|---|---|---|
| Compressive strength | 82. 0 | 69. 8 | 82. 1 | 70. 1 |
| Static flexural strength | 9. 8 | 8. 8 | 10. 5 | 8. 9 |

Since the effects of 3D concrete microstructures with additions of FA/GGBS on the mechanical behavior of HPC have to be comprehensively investigated, the two specimens of 50 mm in length, 50 mm in width and 20 mm in thickness are cut from the central part of each tested concrete specimen for the following micro-CT scan. In order to avoid inducing damage in the concrete bulk by sawing vibrations, each concrete specimen is tightly fixed to the sawing table and is cut slowly by an adamantine saw.

### 1. 2 Micro-CT system and main parameters

A micro-CT system is usually composed of seven main groupwares, i. e. radiation source, detector system, manipulation system, electrical cabinet, radiation protection enclosure, host computer and matching software to capture and analyze 3D scan images. The settings for this study are: 180 kV, 0. 4 mA (X-ray tube current), 3D cone-beam radiation source with a circular source trajectory, a high-resolution planar equispaced detector with a number of 1 024 × 1 024 elements, and reconstructed 3D image of 1 024 × 1 024 × 1 024 pixels in *X*-, *Y*- and *Z*-axis, respectively. The latest micro-CT software and defect detection software are employed for CT system operation, 3D image reconstruction and quantitative analysis. The resolution of each voxel (3D picture element) is 0. 06 mm × 0. 06 mm × 0. 06 mm.

The locations of the radiation source and the planar detector are fixed. Aluminum (Al) and copper (Cu) filters are placed in front of the X-ray source to reduce artifacts. The concrete specimens are installed on the turntable before being scanned. Rotating the turntable in 360°, 1 440 projections (projected images) are obtained for one specimen in the vertical direction. The 3D image of one specimen is reconstructed in 200 s using the combination-weighted Feldkamp-based reconstruction algorithm and the noise filter arithmetic as well as the internal geometrical compensation technique. The gray level in reconstructed images depends on the density contrast among different components: the higher the gray

level, the denser the material. The automatic detection mode of defects is three-dimensional.

## 2 Results and Discussion

### 2.1 Projections and reconstructed 3D images of specimen and defects

During the 360° turning of specimen on the turntable, 1 440 projections in the vertical direction are captured with high resolution by a planar equispaced detector and stored as bitmap files in a host computer. By the combination-weighted Feldkamp-based reconstruction algorithm and the internal geometrical compensation technique, the 3D images of concrete specimens are reconstructed based on the 1 440 projections. An example of a 3D image and a real specimen of S5 are shown in Fig. 1. Except for reflecting different components in the concrete, the 3D image also discovers the heterogenous density distributions of coarse aggregates. Because the computed tomography is established based on the principle of density contrast, some small defects nearly filled with hydration products cannot be separated from the surrounding matrix.

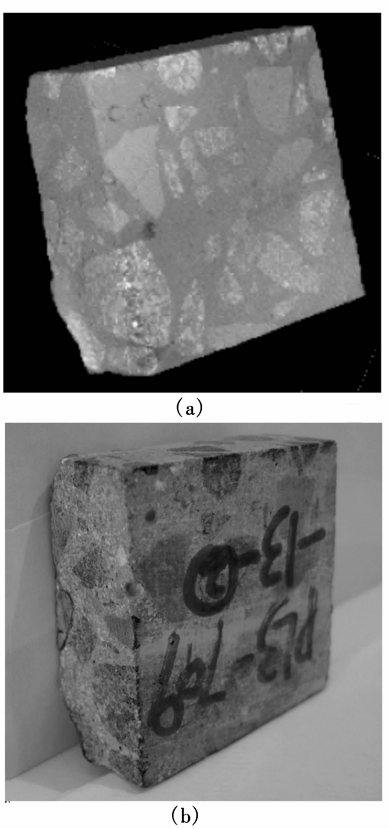


**Fig. 1** Reconstructed 3D image of S5 specimen and the specimen used for micro-CT scan. (a) Reconstructed 3D image of S5 specimen; (b) S5 specimen used for micro-CT scan

The Feldkamp reconstruction of cone-beam data can be formulated as a weighted filtered backprojection[11]. First, the cone-beam projections are individually weighted and ramp is filtered corresponding to the positions of the radiation source. Secondly, the 3D image is reconstructed by the integral algorithm based on weighted projections. The computational cost of a 3D image depends on the projection numbers, pixel numbers in the 3D image and some implementation details such as complexity of the interpolation[11].

A threshold of gray level is automatically chosen for searching defects after comparing the gray level distributions of defects and surrounding materials. Meanwhile, in order to improve the image contrast between defects and surrounding materials, all defects are dyed in a red color. All defects dyed in a red color are solely visualized by filtering the gray levels of the surrounding materials. The spatial images of defects in four tested series are shown in Fig. 2. Since the sand and basalt aggregates are close-grained, the defects shown in Fig. 2 are those existing in the matrix and the aggregate-matrix ITZ. It can be noted that most of the defects in the F3 specimen are fine. Two big flat defects with an irregular shape shown in the spatial image of the F2S3 specimen are cracks in the aggregate-matrix ITZ.

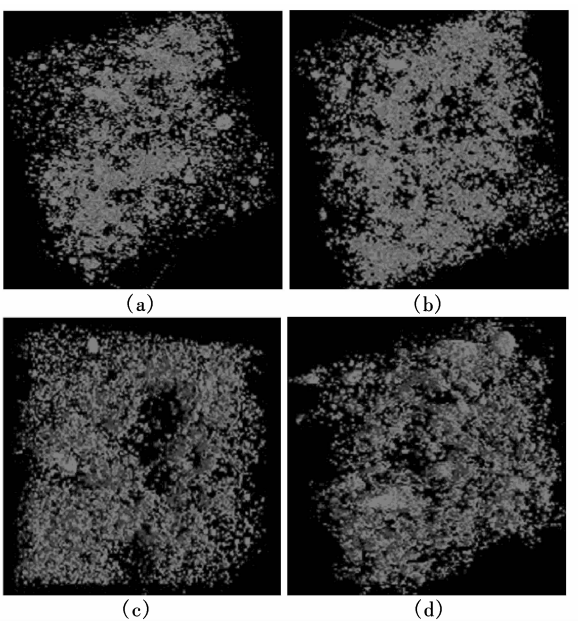


**Fig. 2** Filtered spatial images of defects in four hardened concretes. (a) RC; (b) S5; (c) F3; (d) F2S3

As shown in Fig. 2, the maximum diameters of all noticeable defects in concrete microstructures are obviously different among the four concrete series. The analysis on size of defects is the primary and crucial step for understanding the influences of mineral admixtures on the microstructural and mechanical behaviors of concrete(see Tab. 2).

### 2.2 Defect size distributions

Search and statistical analysis of initial defects in hardened concrete are conducted by the routines in the defect detection software based on the projections of specimens. As is well-known, the quality of projections indeed governs the definition of 3D reconstructed images. Meanwhile, the search and statistics of defects on each projection are helpful for localization and further analysis of each defect in reconstructed 3D images. In order to evaluate the accuracy of micro-CT analysis results, the number and volume distribution of defects are compared with those derived by other methods. According to the volume distributions of defects on different projections, the defect size distributions of the four concrete series are deduced and shown in Fig. 3. It is clearly shown

that the number of defects with a size smaller than 2 $mm^3$ is the major part. For the four tested specimens, the cumulative percentages of the defects with a size smaller than 2 $mm^3$ are 60% to 75% of the total noticeable number of defects.

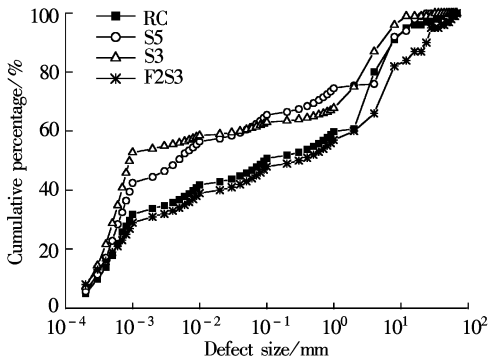


**Fig. 3** Defect size distributions of four tested series

As shown in Fig. 3, 52% and 60% of the total volumes of defects in the F3 specimen correspond to defects with a size smaller than 0.001 $mm^3$ and 0.01 $mm^3$, respectively. These are the highest results in the four tested series. Similarly, 42% and 58% of the total volumes of defects in the S5 specimen correspond to defects with a size smaller than 0.001 $mm^3$ and 0.01 $mm^3$, respectively. For defects in the RC and S5 specimens, the cumulative percentages of defects with a size smaller than 2 $mm^3$ are similar. The volume fractions of defects with a size smaller than 0.001 $mm^3$ in RC and S5 specimens are around 30% of the total defect volumes. The cumulative percentages of defects in the RC specimen with a size from 2 $mm^3$ to 10 $mm^3$ obviously increase. It is obvious that the admixtures of fly ash and ground slag in concrete significantly increase the volume fractions of defects with a size smaller than 0.001 $mm^3$.

## 2.3 Volume fractions of defects

The volume fractions of defects in the four concrete series are conveniently calculated and listed in Tab. 3. It should be noted that the defects detected by the threshold-based method include the microscopic cracks and voids in the hardened concrete. Therefore, it is noted that the volume fractions of defects in hardened concrete are different from the air contents in fresh paste of concrete[1].

**Tab. 3** Analysis results of defect volume fractions based on 3D images %

| Noticeable defect size/$mm^3$ | RC | S5 | F3 | F2S3 |
|---|---|---|---|---|
| ≥0.000 2 | 1.52 | 1.65 | 1.85 | 2.34 |

Combining 3D defect images in Fig. 2 with volume fractions of defects in Tab. 3, it is obvious that the qualitative observation on the defect density is consistent with the quantitative analysis results of defect volume fractions. Moreover, based on the results in Fig. 3 and Tab. 3, we can also conclude that: 1) Addition of 30% fly ash makes the defects finer than those in RC, but the defect volume fraction is slightly higher than that of RC; 2) Addition of ground slag with a 50% mass fraction of total cementitious materials does not greatly increase the volume fractions of defects, but the amount of defects with a size smaller than 0.001 $mm^3$ is greater than that in RC; 3) The combined addition of fly ash and ground slag in concrete obviously decreases the total number of defects in hardened concrete, but the amount of defects with a size larger than 2 $mm^3$ is increased.

Since the whole analysis on defects is performed by quantification of voxels distributed in 3D images, the volume fractions of defects can be linked to the analysis results of thin sections on 2D images[12]. In order to confirm the accuracy of previous analysis results, the volume fractions of defects on a series of 2D images are also analyzed with the recommended method in ASTM-C457[3]. All of the defects are detected from 2D images by Matlab-R2006a code based on the threshold gray value of defects. Ten continuous slices of constant thickness in each specimen are taken to reduce the statistical uncertainty of this method. Moreover, in order to further evaluate the accuracy of the calculation results of noticeable defects based on 3D/2D images, the porosities of concrete specimens used for CT scanning are conducted by water-suction tests with a negative pressure of 4 kPa for 24 h. The mean volume fractions of noticeable defects in the four series specimens respectively calculated by CT software, Matlab program and water-suction tests are plotted in Fig. 4.

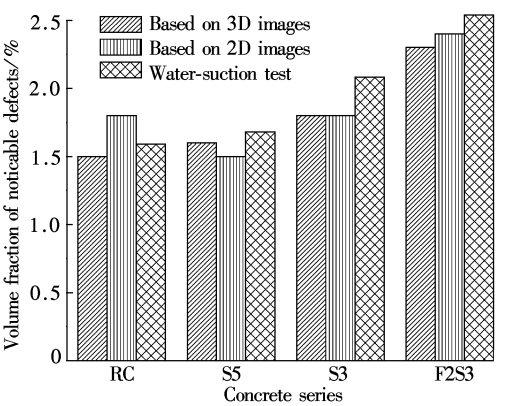


**Fig. 4** Volume fractions of noticeable defects based on 3D/2D image analysis and suction pressure test

It can be deduced from Fig. 4 that the defect volume fractions of hardened concretes (except RC), performed by 3D/2D image analysis and water-suction tests, are similar to each other. The differences in the results of RC are less than 5%. The results of defect volume fractions in RC based on 2D images are about 3% higher than those of the water-suction test. For the other specimens, the results based on the 3D/2D image analysis are slightly less than those based on the water-suction test. One of the reasons for these differences is that the gray value of some voids in the 3D images is influenced by filled hydration products inside (see Fig. 5). These filled hydration products can decrease the automatic analysis results of the total volume fractions of defects using CT software based on the mean gray value of cracks and voids. Furthermore, because the porosities with a diameter of more than 0.5 nm can be permeated by water molecules[2], the micro-porosity with a size of less than 0.06 mm × 0.06 mm × 0.06 mm (i.e. the resolution of a voxel in 3D image of proposed micro-CT) in this case can be measured with water-suction tests. However, because the volume fractions of defects with a size smaller than 0.06 mm × 0.06

mm × 0.06 mm in concrete are greatly fewer than those of larger defects in concrete, the volume fractions of noticeable defects in the four specimens tested by water-suction tests are only slightly higher than those analyzed with 3D/2D images. Unfortunately, though the water-suction test is a simple and cheap method compared with the functions of the 3D micro-CT system, the diameter distributions and spatial images of defects in the hardened concrete microstructure cannot be displayed. It is the uppermost disadvantage of this test.

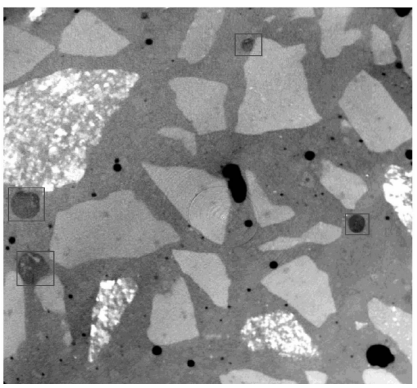

**Fig. 5** An example of voids nearly filled by hydration products( see square marks)

## 3 Conclusion

The experimental findings shown in the present paper have identified that the micro-CT system is helpful in investigating the effects of mineral admixtures on the concrete internal features as well as to comprehensively understand the influences of spatial distributions and volume fractions of defects on the mechanical behavior of concrete structures. The differences among the spatial information of defects in the four series of specimens are mainly caused by the material components in the concrete matrix when the water-to-binder ratio and the size distribution of aggregates are constant. Furthermore, the analysis results of defects are helpful in proving that the additions of Class F fly ash and S95 ground slag obviously change the mean size and the volume fraction of defects in hardened concrete by their grain-filling effect and pozzolanic effect. The additions of fly ash and ground slag increase the number of defects with a volume of less than 0.001 $mm^3$. For the concrete with combination of fly ash and ground slag, the cumulative volume fractions of defects with a volume larger than 2 $mm^3$ obviously increase. Since the concrete fracture is not only controlled by the spatial distribution of defects but also by the strengths of the matrix and matrix-aggregate interfacial zones, the differences in the mechanical properties of HPC with different dosages of fly ash and/or ground slag can be quantitatively explained to a certain extent by the defect analysis results shown in the present paper.

Although the volume fractions of defects tested by the water-suction method and the X-ray micro-CT system are quite close to each other, the latter method is un-substitutable by the former one for precise research on the effects of the spatial geometry and diameter distribution of defects on the mechanical behaviors of hardened concrete.

Acknowledgements The authors gratefully acknowledge the assistance of YXLON Int. X-Ray GmbH. The first author specially acknowledges discussion with M. Münker and B. Muerkens, and raw data supplied by M. Harbecke.

## References

[1] Wong R C K, Chau K T. Estimation of air void and aggregate spatial distributions in concrete under uniaxial compression using computer tomography scanning [J]. *Cement and Concrete Research*, 2005, **35**(8): 1566 − 1576.

[2] Galle C. Effect of drying on cement-based materials pore structure as identified by mercury intrusion porosimetry — a comparative study between oven-, vacuum-, and freeze-drying [J]. *Cement and Concrete Research*, 2001, **31**(10): 1467 − 1477.

[3] ASTM. ASTM-C457—98 Standard test method for microscopical determination of parameters of the air-void system in hardened concrete [S]. USA: American Society for Testing and Materials, 1998.

[4] Bejaoui S, Bary B. Modeling of the link between microstructure and effective diffusivity of cement pastes using a simplified composite model [J]. *Cement and Concrete Research*, 2007, **37**(3): 469 − 480.

[5] Leite J P B, Slowik V, Mihashi H. Computer simulation of fracture processes of concrete using mesolevel models of lattice structures [J]. *Cement and Concrete Research*, 2004, **34**(6): 1025 − 1033.

[6] Carpinteri A, Spagnoli A. A fractal analysis of size effect on fatigue crack growth [J]. *International Journal of Fatigue*, 2004, **26**(2): 125 − 133.

[7] Van Geet M, Swennen R, Wevers M. Quantitative analysis of reservoir rocks by microfocus X-ray computerised tomography [J]. *Sedimentary Geology*, 2000, **132**(1/2): 25 − 36.

[8] Flannery B P, Deckman H W, Roberge W G, et al. Three-dimensional X-ray microtomography [J]. *Science*, 1987, **237**(4821): 1439 − 1444.

[9] Landis E N, Nagy E N, Keane D T, et al. Technique to measure 3D work-of-fracture of concrete in compression [J]. *Journal of Engineering Mechanics*, 1999, **125**(6): 599 − 605.

[10] Zhang T, Nagy G, Nagy E N, et al. Three-dimensional analysis of crack geometry [C]//*Proceedings of the* 6*th International Conference on Fracture Mechanics of Concrete and Concrete Structures — New Trends in Fracture Mechanics of Concrete*. Catania, Italy, 2007: 77 − 84.

[11] Mori S, Endo M, Komatsu S, et al. A combination-weighted Feldkamp-based reconstruction algorithm for cone-beam CT [J]. *Physics in Medicine and Biology*, 2006, **51**(16): 3953 − 3965.

[12] Li Y X, Chen Y M, Wei J X, et al. A study on the relationship between porosity of the cement paste with mineral additives and compressive strength of mortar based on this paste [J]. *Cement and Concrete Research*, 2006, **36**(9): 1740 − 1743.

[13] Sun W, Zhang Y S, Liu S F, et al. The influence of mineral admixtures on resistance to corrosion of steel bars in green high-performance concrete [J]. *Cement and Concrete Research*, 2004, **34**(10): 1781 − 1785.

[14] Maso J C. *Interface transition zone in concrete*[M]. UK: St Edmundsbury Press, 1996: 103 − 115.

# 基于三维微焦点 CT 图像对高性能混凝土内部缺陷的测量和分析

郭丽萍[1,2] Andrea Carpinteri[3] 孙 伟[1,2] 秦文超[4]

([1]东南大学材料科学与工程学院,南京 211189)
([2]东南大学江苏省土木工程材料重点实验室,南京 211189)
([3]帕尔马大学土木工程系,意大利帕尔马 43100)
([4]德国依科视朗国际射线有限公司上海代表处,上海 200041)

**摘要**:为了揭示粉煤灰和磨细矿渣对混凝土微观结构初始缺陷的影响规律,采用高分辨率 X-射线微焦点 CT(X-ray Micro-CT)图像对具有不同胶凝材料的 4 个系列高性能混凝土进行了研究. 混凝土微观结构和缺陷过滤之后的高分辨率三维图像均由 Micro-CT 配套的图像软件进行了重建. 基于二维和三维图像分析得到了混凝土内部缺陷的尺寸分布和体积分数,并与常温饱水法的试验结果进行了对比. 研究结果显示:矿物掺和料作为胶凝材料加入混凝土之后,由于其颗粒填充效应和火山灰效应,显著改变了硬化混凝土的微观结构特征以及初始缺陷的尺寸和空间分布特征;在水胶比和集料尺寸分布保持不变的条件下,矿物掺和料的掺入与否,是引起高性能混凝土展示出不同力学特性的主要原因.

**关键词**:高性能混凝土;缺陷;微观结构;X-射线微焦点 CT;矿物掺和料
**中图分类号**:TU522. 07